Supporting Information

Zhang et al. 10.1073/pnas.1019051108

SI Methods

Materials. The *Escherichia coli* signal recognition particle (SRP) and SRP receptor (SR) GTPases (Ffh and FtsY, respectively) and the 4.5S RNA were expressed and purified as described previously (1, 2). All the experiments in this work used SRP, which is the complex of Ffh bound to the 4.5S RNA. Truncated FtsY (47–497) was used in all the fluorescence and EPR measurements except for the charge reversal mutant FtsY (RRLRR). The abilities of FtsY (47–497) to interact with SRP and respond to the cargo are similar to those of full length FtsY (1). Mutant Ffh and FtsYs were constructed using the QuickChange mutagenesis procedure (Stratagene). All the mutant proteins were expressed and purified using the same procedure as that for the wild-type proteins. Fluorescent dyes N-(7-dimethylamino-4-methylcoumarin-3-yl)maleimide (DACM) and BODIPY-FL-N-(2-aminoethyl)-maleimide were from Invitrogen.

RNC_{FtsQ} Purification. Homogeneous RNC_{FtsQ} was generated from in vitro translation using membrane free cell extract prepared from MRE600 cells and was purified by affinity chromatography and sucrose gradient centrifugation as described previously (3, 4). Purified RNC_{FtsQ} serves as a functional cargo in protein targeting because it can bind SRP, trigger factor, and the secYEG translocon complex (4). In quantitative assays, purified RNC_{FtsQ} exhibited the same affinity for SRP as those measured with RNCs that do not contain an affinity tag (5).

Fluorescence Labeling. For FRET measurements, DACM and BODIPY-FL were used to label single-cysteine mutants of Ffh and FtsY, respectively, as described previously (2). Labeled protein was purified as described (2), and the efficiency of labeling was typically ≥95% with a background of <5%.

Spin Labeling. Single-cysteine mutants of FtsY [in 20 mM HEPES (pH 8.0), 150 mM NaCl and 2 mM EDTA] were incubated with a 10-fold molar excess of dithiothreitol (DTT) at room temperature for 1–2 h to reduce any disulfide bonds. DTT was removed by gel filtration chromatography. The reduced and degassed proteins (approximately 100μM) were labeled with a 3- to 5-fold molar excess of methanethiosulfonate spin label (MTSSL) (Toronto Research Chemicals) at room temperature in the dark for 2–3 h. Excess MTSSL was removed by gel filtration chromatography. The labeling efficiency was determined by EPR using the TEMPO calibration curve (Bruker user manual), and was typically >80% with <5% background as assessed from the cysteineless wild-type protein using the same procedure. All the spin-labeled proteins were tested for interaction with SRP using the GTPase assay; only the spin-labeled FtsY mutants that did not substantially disrupt activity were used for EPR measurements.

EPR Conditions. EPR measurements were carried out in SRP buffer [50 mM KHEPES, pH 7.5, 150 mM KOAc, 2 mM Mg(OAc)$_2$, 2 mM DTT, 0.01% Nikkol] to determine the local mobility of 23 spin-labeled FtsY mutants in apo-FtsY, in the early intermediate, and in the stable complex. For apo-FtsY, 75–100 μM spin-labeled protein was used to obtain the EPR spectra. The early intermediate was formed by mixing 30 μM spin-labeled FtsY with 90 μM SRP in the presence of GDP. Based on the affinity of the early intermediate ($K_d \sim 4$–10 μM) (2), >90% of labeled FtsY formed the early complex with SRP under these conditions. The stable complex was formed by mixing 30 μM spin-labeled-FtsY with 60 μM SRP in the presence of 5′-guanylylimido-diphosphate (GMPPNP). Over 99% of labeled FtsY formed a stable complex with SRP under these conditions, according to the K_d values of the stable complex of approximately 16–30 nM (2).

Time-Resolved (TR)-FRET Conditions. Donor-only measurements were carried out in SRP buffer in the presence of 5 or 1 μM DACM-labeled SRP for the early and stable complexes, respectively. For the early intermediate, 5 μM DACM-labeled SRP and 50 μM BODIPY-FL–labeled SR were mixed together in the presence of GDP. For the stable complex, 1 μM DACM-labeled SRP and 8 μM BODIPY-FL–labeled SR were mixed in the presence of GMPPNP. Under these conditions, formation of both complexes was complete after a 20-min incubation at room temperature in dark.

Numerical Analysis for TR-FRET Measurements. The measured short and long timescale data were spliced together, and the combined traces were compressed logarithmically before the fitting process (70 points per decade). The splicing and compression did not introduce artifacts to the interpretation of data (6). Analyses of the TR-FRET data can be described as a numerical inversion of a Laplace transform $[I(t) = \sum_k P(k) \exp^{-kt}]$, in which $I(t)$ is fluorescence intensity, k is the fluorescence decay rate constant, and $P(k)$ is the probability of a specific k (7, 8). In this work, two algorithms were used to invert the kinetics data with regularization methods that also impose a nonnegativity constraint, $P(k) \geq 0$ ($\forall k$). The first method, based on the least-squares (LSQ) fitting, used a MATLAB algorithm (LSQNONNEG) (Mathworks) that minimizes the sum of the squared deviations (χ^2) between observed and calculated values of $I(t)$, subject to the nonnegativity constraint. This algorithm produces the narrowest $P(k)$ distributions and smallest values of χ^2 with relatively few nonzero components. The second method is based on the maximum entropy (ME) theory. The information theory proposes that the least-biased solution to the inversion problem is to minimize χ^2 and maximize the breadth of $P(k)$ (9). This regularization condition can be met by maximizing the Shannon–Jaynes entropy of the rate-constant distribution $\{S = -\sum_k P(k) \ln[P(k)]\}$ while satisfying the nonnegativity constraint. ME fitting generated stable and reproducible numerical inversions of the kinetics data. The balance between χ^2 minimization and entropy maximization is evaluated by the L-curve analysis, which yielded upper limits for the widths of $P(k)$ consistent with experimental data. The $P(k)$ distributions from ME fitting were broader than those obtained with LSQ fitting but exhibited maxima at similar locations.

Both methods were used to generate the decay rate distribution $P(k)$. A coordinate transformation using the Förster relation (Eq. **S1**) was then used to convert the probability distribution of the decay rates k to the donor–acceptor distances r, thus generating the donor–acceptor distance distribution $P(r)$:

$$r = R_0 \left(\frac{k}{k_0} - 1 \right)^{1/6}. \qquad \textbf{[S1]}$$

The Förster radius, R_0, for the DACM/BODIPY-FL pair is approximately 47 Å. The value of k_0 was obtained from donor-only measurements, which gave a nearly single-exponential (>90%) fluorescence decay kinetics for all three positions in this study. At distances larger than 1.5 R_0, energy transfer does not take place efficiently, whereas at distances less than approximately 13 Å, the Förster model does not reliably describe FRET kinetics. Therefore, our TR-FRET measurements can provide

information about donor–acceptor distances only in the range of 13–70 Å.

Fluorescence Anisotropy Measurements. Anisotropy measurements used excitation and emission wavelengths of 380 and 470 nm for DACM and 450 and 518 nm for BODIPY, respectively. Fluorescence anisotropy was calculated according to Eq. **S2**:

$$R = \frac{(I_{VV} - G \times I_{VH})}{(I_{VV} + 2G \times I_{VH})},$$ [S2]

in which I_{VV} and I_{VH} are the vertically and horizontally polarized emission intensities when the sample is vertically excited, and G is the grating factor that corrects for the wavelength response to polarization of the emission optics and detectors, defined as $G = I_{HV}/I_{HH}$, where I_{HV} and I_{HH} are the vertically and horizontally polarized emission intensities when the sample is horizontally excited.

Contribution of Dipole Orientation and Fluorophore Linkers to Distance Distribution. Fluorescence anisotropy measurements showed that both the donor and acceptor fluorophores exhibited low anisotropy values comparable to the free dye when they were incorporated into the proteins (Table S1). This strongly suggests that the labeled fluorophores are relatively free rotamers with randomized orientations. Hence, the orientation factor, κ^2, can be approximated by $\langle\kappa\rangle^2 = 2/3$. In addition, the distance distribution can be widened and/or shifted by the fluorophore linkers. For DACM, the linker length is short and very rigid; thus, the primary contribution of the linker is to shift the measured distances by approximately 5 Å. BODIPY-FL has a long (six carbon bonds) and flexible linker that will widen the distance distribution. This effect was estimated as one effective Gaussian chain with the parameter, $r^{\text{linker}} = \sqrt{L \times l_p}$, in which L and l_P are the contour and persistence lengths of the fluorescence linker, respectively (10). This yielded an estimated r^{linker} value of approximately 7 Å for BODIPY-FL. Molecular docking simulations confirmed that the fluorophore linkers caused less than 7 Å deviations in the measured distances.

GTPase Assay. The assay to measure the stimulated GTP hydrolysis reaction between SRP and SR was performed and analyzed as described (1). Briefly, reactions were carried out in SRP buffer in the presence of a small, fixed amount of SRP (100–200 nM), varying amounts of SR, and saturating GTP (100–200 μM). The observed rate constants (k_{obsd}) were plotted against SR concentration and fit to Eq. **S3**,

$$k_{\text{obsd}} = k_{\text{cat}} \times \frac{[\text{SR}]}{K_m + [\text{SR}]}$$ [S3]

in which k_{cat} is the maximal rate-constant at saturating SR concentrations, and K_m is the concentration required to reach half saturation. Because k_{cat} is at least 100-fold faster than the rate of SRP•SR complex disassembly, the rate constant k_{cat}/K_m in this assay is rate-limited by and therefore equal to the rate of stable SRP•SR complex formation (1). No DTT was present in the reactions involving spin-labeled proteins.

Docking. The ClusPro 2.0 docking server was used to generate docking models for the early intermediate (11). This program was chosen because it emphasizes the number of energy-preferred structures in the docking cluster and is therefore particularly suitable to generate an ensemble of conformations for the early intermediate. During the docking, *E. coli* Ffh was set as a static receptor while *E. coli* FtsY was set as a ligand that searched for the best docking position with the receptor.

The initial docking positions were generated by the fast Fourier transform method without using the FRET distances as constraints; and the resulting docking positions were clustered according to their root-mean-square deviations. The best energy conformations were sorted as clusters via a filter that was set to an energy function that favors electrostatic interactions. The ranking of the clusters was determined by the number of structures that each cluster contained. The top five clusters had 89, 88, 65, 59, and 46 structures, respectively. The top two clusters, named "G" and "N," were chosen for further analyses.

Brownian Dynamics. BrownDye was used for Brownian dynamics calculations (12). Adaptive Poisson–Boltzmann solver was used to calculate the electrostatic potentials (13). Partial atomic charges and atomic radii were assigned from the PARSE parameter set. The dielectric constants were assigned to be 4 in the protein interior and 78 in the exterior. Grids were assigned with dimensions of $193 \times 193 \times 193$ points. Temperature was set to 298 K, and ionic strength was set to 100 mM. Brownian dynamics trajectories were started at a minimum intermolecular separation that still gave spherically symmetric forces. The number of trajectories to estimate the association rate constants varied from 40,000 to 100,000 depending on how fast the rates were. The reaction criterion was specified by the atom-contact pairs defined by the structure of the complex. All the intermolecular nitrogen–oxygen pairs within 0.55 nm were considered as within the reaction criterion. A series of simulations with different levels of reaction criteria were generated by systematically tuning the required atom-contact number from 3 to 7. Three structures were used for this analysis to obtain the association rate constants: the central structure of the G cluster, the central structure of the N cluster, and the crystal structure of the stable complex.

1. Peluso P, Shan SO, Nock S, Herschlag D, Walter P (2001) Role of SRP RNA in the GTPase cycles of Ffh and FtsY. *Biochemistry* 40:15224–15233.
2. Zhang X, Kung S, Shan SO (2008) Demonstration of a multistep mechanism for assembly of the SRP•SRP receptor complex: Implications for the catalytic role of SRP RNA. *J Mol Biol* 381:581–593.
3. Zhang X, Schaffitzel C, Ban N, Shan SO (2009) Multiple conformational switches in a GTPase complex control co-translational protein targeting. *Proc Natl Acad Sci USA* 106:1754–1759.
4. Schaffitzel C, Ban N (2007) Generation of ribosome nascent chain complexes for structural and functional studies. *J Struct Biol* 158:463–471.
5. Bornemann T, Jockel J, Rodnina MV, Wintermeyer W (2008) Signal sequence-independent membrane targeting of ribosomes containing short nascent peptides within the exit tunnel. *Nat Struct Mol Biol* 15:494–499.
6. Kimura T, Lee JC, Gray HB, Winkler JR (2009) Folding energy landscape of cytochrome cb562. *Proc Natl Acad Sci USA* 106:7834–7839.
7. Beals JM, Haas E, Krausz S, Scheraga HA (1991) Conformational studies of a peptide corresponding to a region of the C-terminus of ribonuclease A: Implications as a potential chain-folding initiation site. *Biochemistry* 30:7680–7692.
8. Beechem JM, Haas E (1989) Simultaneous determination of intramolecular distance distributions and conformational dynamics by global analysis of energy transfer measurements. *Biophys J* 55:1225–1236.
9. Istratov AA, Vyvenko OF (1999) Exponential analysis in physical phenomena. *Rev Sci Instrum* 70:1233–1257.
10. Laurence TA, Kong X, Jager M, Weiss S (2005) Probing structural heterogeneities and fluctuations of nucleic acids and denatured proteins. *Proc Natl Acad Sci USA* 102:17348–17353.
11. Kozakov D, et al. (2010) Achieving reliability and high accuracy in automated protein docking: ClusPro, PIPER, SDU, and stability analysis in CAPRI rounds 13–19. *Proteins* 78:3124–3130.
12. Ermak DL, McCammon JA (1978) Brownian dynamics with hydrodynamic interactions. *J Chem Phys* 69:1352–1360.
13. Baker NA, Sept D, Joseph S, Holst MJ, McCammon JA (2001) Electrostatics of nanosystems: Application to microtubules and the ribosome. *Proc Natl Acad Sci USA* 98:10037–10041.
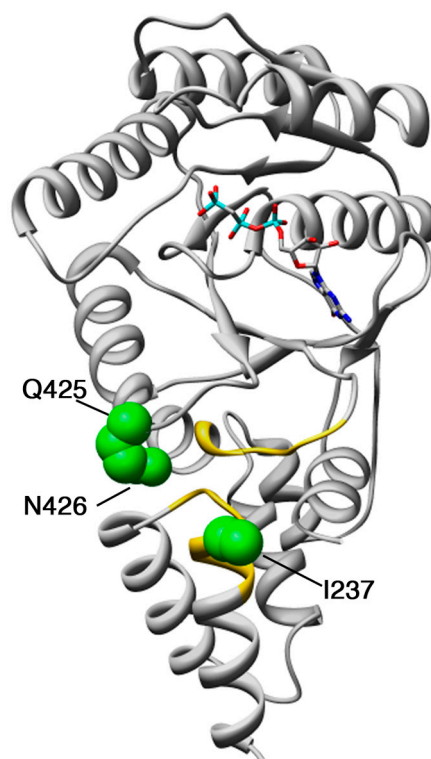
Fig. S1. The mobility of spin labels on SR changed upon formation of the early intermediate, stable complex, or both. (*A* and *B*) Spin-labeled SR were screened using the GTPase assay. The activities of spin-labeled (SL) SRs in interaction with SRP were analyzed using the GTPase assay (see *SI Methods*). Two kinetic parameters were assessed: the GTPase rate constants of the SRP•SR complex (k_{cat} in *A*) and the association rate constants for stable SRP•SR complex assembly (as determined by k_{cat}/K_m in *B*; see *SI Methods*). Spin-labeled SR's that were defective in either property by a factor of 5 or more were not used for EPR studies (open bars). Only the spin-labeled SR's that were functional in interacting with SRP (gray bars) were used for EPR measurements shown in *C* and *D*. (*C*) Spectra of additional spin probes in SR that changed mobility upon formation of either the early intermediate or the stable complex. Three different classes were defined in the text based on probe mobility changes. The mobility of spin label was analyzed from the central line width (ΔH_0) and the breadth of the spectra, and are summarized in Fig. 1*B*. Black, blue, and red denote the free protein, the early intermediate, and the stable complex, respectively. (*D*) EPR spectra of spin probes in SR that exhibited no significant changes in mobility upon formation of either complex. Color-coding is the same as in *C*.

Fig. S2. Residues I237, Q425, and N426 (green), which changed EPR spectra specifically in the stable complex, are at the conserved motifs (yellow) that mediate NG-domain rearrangement.
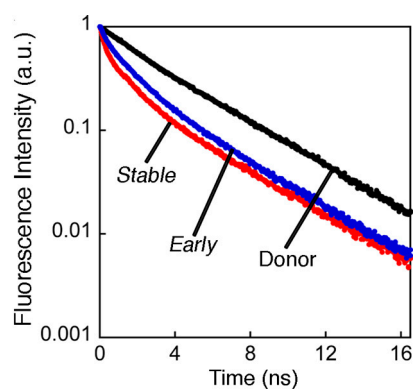

Fig. S3. Fluorescence decay of donor (DACM)-labeled SRP (C76) under different experimental conditions. The black, blue, and red curves represent the decay curves for donor-only, the early intermediate, and the stable complex, respectively. The linear decay of the donor-only sample could be described by a single decay rate constant. In contrast, the decay curves in both the early intermediate and stable complex deviated from linearity and were described by multiple decay rate constants.
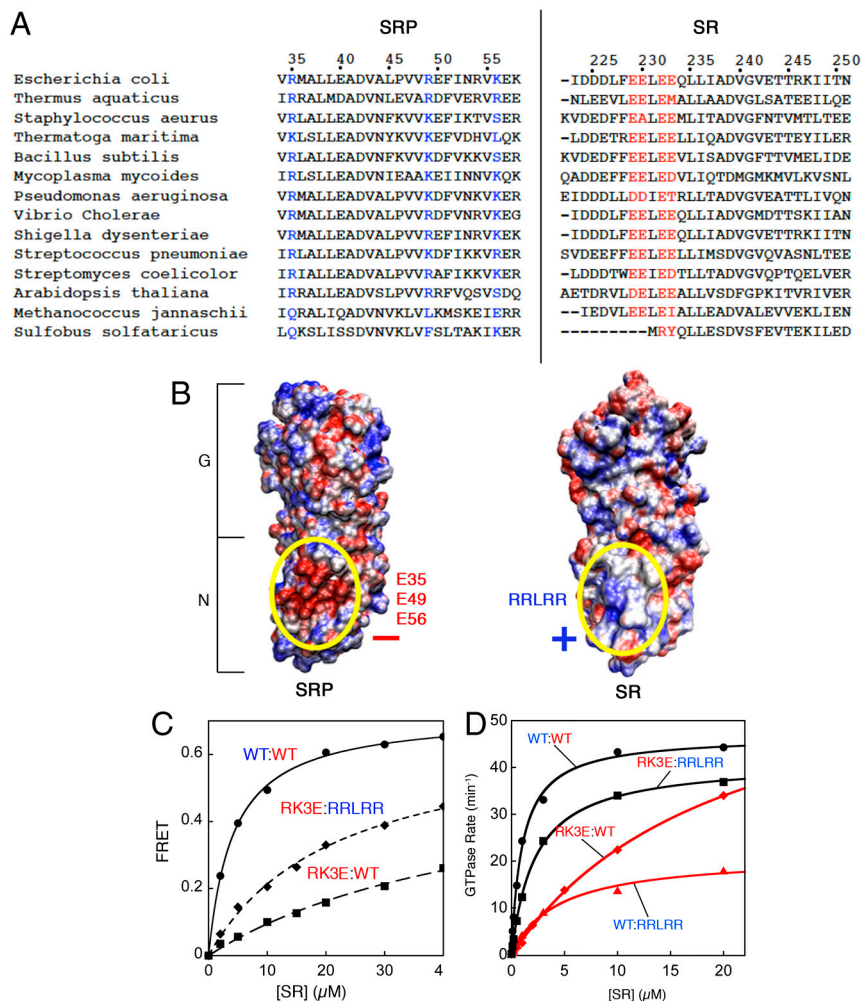
Fig. S4. Distance distributions derived from least-squares analyses of the TR-FRET data for each FRET pair in the early intermediate (blue), stable complex (red), and early intermediate bound with cargo (green).

Fig. S5. Charge complementarity between N domains of SRP and SR are essential for the stability of the early intermediate and the kinetics of stable complex assembly. (*A*) Sequence alignment of SRP and SR homologues. The residue numbering is for the *E. coli* SRP and SR proteins. Conserved positive and negative residues are denoted in blue and red, respectively. (*B*) The R36E:R49E:K56E (RK3E) mutation in SRP generated a negatively charged surface in the SRP N domain (*Left*), and the RRLRR mutation in SR generated a moderately positively charged surface in the SR N domain (*Right*). (*C*) The stabilities of the early intermediates formed by mutant SRP and SRs were determined by equilibrium titrations. Nonlinear fits of data to Eq. **1** (main text) gave K_d values of 4.0 μM for WT:WT (wild-type SRP and SR), 50.1 μM for RK3E:WT [mutant SRP (RK3E) and wild-type SR], and 20.1 μM for RK3E:RRLRR [mutants SRP (RK3E) and SR (RRLRR)]. (*D*) The kinetics of stable complex assembly, determined using the GTPase assay as described in *SI Methods*. Nonlinear fits of the data gave k_{cat}/K_m values of 0.72×10^6, 0.056×10^6, 0.080×10^6, and 0.31×10^6 M^{-1} s^{-1}, respectively, for the interaction between the wild-type proteins (WT:WT), wild-type SRP and mutant SR (WT:RRLRR), mutant SRP and wild-type SR (RK3E:WT), and the charge reversal SRP and SR mutants (RK3E:RRLRR).
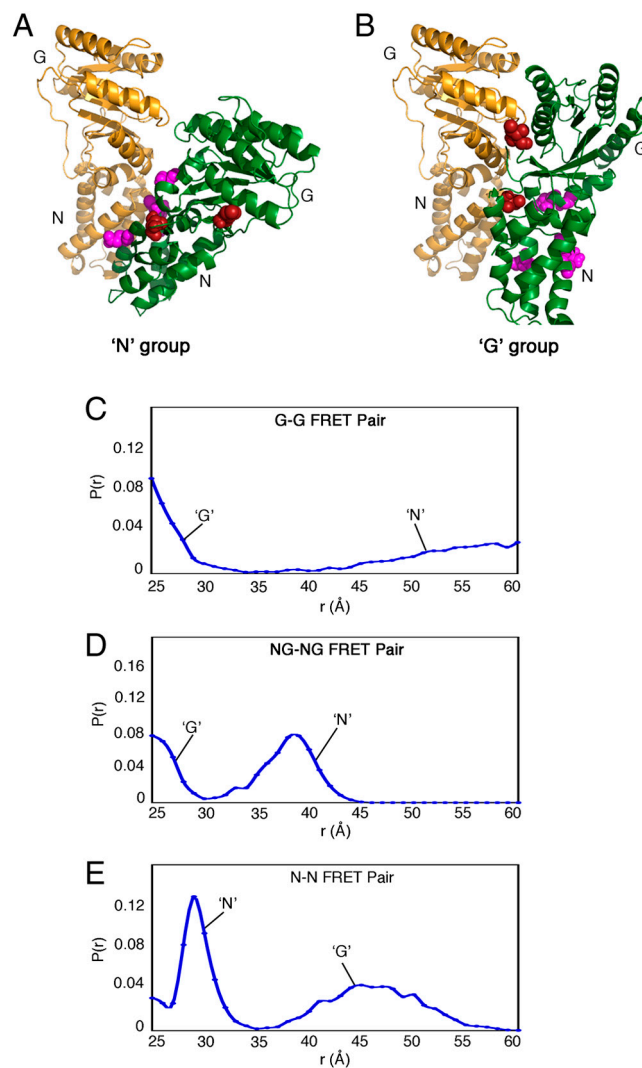
Fig. S6. The N and G groups represent possible conformations within the ensemble of the early intermediate. (*A* and *B*) Spin probes that changed mobility upon formation of the early intermediate are close to the interaction surface of either the N (magenta residues) or the G (red residues) group. The SRP NG domain is in gold, and the SR NG domain is in green. (*C–E*) Distance distributions of the three pairs of FRET probes predicted by a combination of the docking structures in the N and G groups.
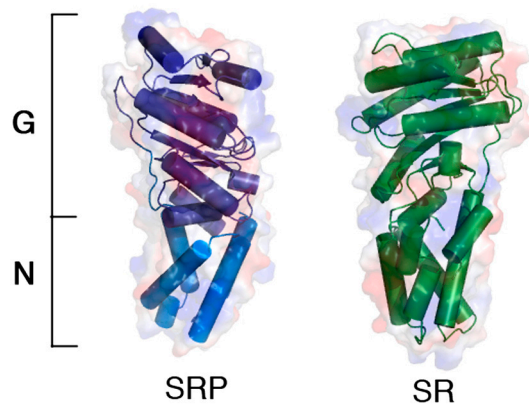
Movie S1. SRP•SR assembly: This movie summarizes the complex assembly process between the SRP and SR GTPases based on information from biochemical, biophysical, and crystallographic analyses and molecular docking simulations.
Movie S1 (MOV)

Table S1. Anisotropy measurement for DACM and BODIPY-FL fluorophores

	DACM	DACM SRP C173	DACM SRP C235	DACM SRP C76
Anisotropy	0.09188	0.09494	0.12368	0.05234
	BODIPY	BODIPY SR C345	BODIPY SR C487	BODIPY SR C242
Anisotropy	0.03232	0.05752	0.09678	0.07122